






Fully Automated CAD System for Lung Cancer Detection and Classification Using 3D Residual U-Net with multi-Region Proposal Network (mRPN) in CT Images

Anum Masood^{1,2}, Usman Naseem³, and Mehwish Nasim^{4,5,6}

¹ Department of Nuclear Medicine, RWTH University Hospital, Aachen, Germany

² Institute of Neuroscience and Medicine (INM-2),
Forschungszentrum Jülich, Jülich, Germany
a.masood@fz-juelich.de

³ College of Science and Engineering, James Cook University, Townsville, Australia
usman.naseem@jcu.edu.au

⁴ College of Science and Engineering, Flinders University, Adelaide, Australia

⁵ School of Computer and Mathematical Sciences,
University of Adelaide, Adelaide, Australia

⁶ School of Physics, Mathematics, and Computing,
University of Western Australia, Adelaide, Australia
mehwish.nasim@uwa.edu.au

Abstract. Lung cancer is one of the leading causes of mortality worldwide. The survival rate of lung cancer depends on its timely detection and diagnosis. For pulmonary cancer detection, numerous Computer-Assisted Diagnosis (CADx) systems have been developed that use the CT scan imaging modality. Recent advancement in deep learning techniques has enabled these CADx to automatically model high-level abstractions in CT-Scan images using a multi-layered Convolutional Neural Network (CNN). Our proposed CAD system comprises 3D residual U-Net for nodule detection. Initially, the 3D residual U-Net resulted in false positive results; therefore, a multi-Region Proposal Network (mRPN) was proposed for the improvement of nodule detection. The detected nodules are assigned a probability of malignancy. Furthermore, each detected nodule is classified into four classes based on its respective malignancy score. Extensive experimental results illustrate the effectiveness of our 3D residual U-Net model. These results demonstrate the exceptional detection performance achieved by our proposed model with a sensitivity of 97.65% and an average classification accuracy of 96.37%. Performance analysis demonstrates the potential of the proposed CAD system for the detection and classification of lung nodules with high efficiency and precision.

Keywords: CT image · Lung cancer · CAD systems · Deep Learning · 3D U-Net

1 Introduction

Lung cancer has the highest mortality rate in both males and females where the 3-year survival rate for patients with lung cancer is 25% [19]. There are no obvious symptoms at the beginning of lung cancer, and as a consequence, most patients seek treatment at the later stage, minimizing survival chances. Therefore, early detection and diagnosis of lung cancer is of the utmost importance [1]. The chest computed tomography (CT) imaging modality provides high-resolution images of nodules with lavish details; however, pulmonary nodules have inhomogeneous densities and lower contrast compared to blood vessel segments and other anatomical structures, increasing the complexity of nodule detection [2, 12]. To assist radiologists in automatically detecting nodules and replacing the time-consuming manual delineation of nodules, Computer-Aided Detection (CADe) and Diagnosis (CADx) systems are developed. The latest technologies use Artificial Intelligence (AI) to assist in the auxiliary diagnosis of the disease and improve the overall accuracy of the diagnosis while decreasing the detection time [10]. In recent literature, researchers have presented deep learning-based CAD systems with promising results. The convolutional neural network (CNN) framework has been used for the classification of nodules [7] and the reduction of false positive (FP) [20]. Shen et al. proposed a Multi-Crop CNN (MC-CNN) [18] and Setio et al. developed Multi-View CNN (MV-CNN) [16] to classify lung nodule. A 3D-CNN model based on Volumes of Interest (VOI) and a Fully Convolutional Network (FCN) was used to produce a score map for nodule classification [9]. Both CADe and CADx systems have been independently investigated [6], CADe are unable to provide lesion’s radiological characteristics, consequently missing crucial information, while CADx systems do not identify lesions and therefore do not possess high levels of automation. Therefore, a new and advanced CAD system is needed that incorporates the benefits of detection from CADe and diagnosis from CADx into a single system for better performance.

1.1 Contribution

Our contribution is as follows:

- **3D Residual U-Net Model** A novel nodule detection method is proposed using 3D CT images for candidate nodule detection; compared to existing 2D U-Net models, our 3D residual model considers rich spatial features and therefore has more discriminative selection criteria.
- **Multi-Region Proposal Network (mRPN)** We added four RPNs so that nodules with varying diameters can be detected with ease and efficiency. The RPN split-and-merge cascade network mitigates the problem of undetected small nodules.
- **Malignancy Score-Based Approach (MSBA)** Malignancy score is calculated to classify each detected nodule into one of the four classes based on its aggregate malignancy score.

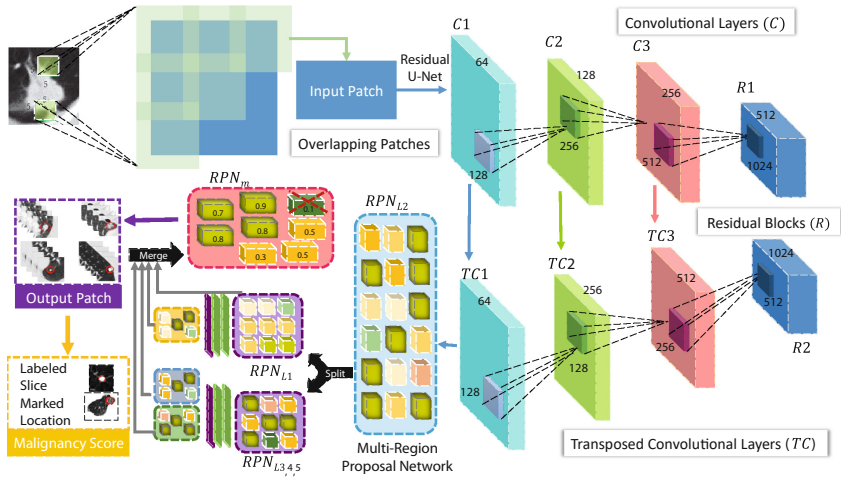


Fig. 1. Overview of our CAD system comprising of 3D residual U-Net and multi-Region Proposal Network for lung nodule detection and classification.

- **False-Positive Reduction Algorithm (FPRA)** We proposed an algorithm for a false positive (FP) reduction rate. Comparative results are much better than the existing FP reduction algorithm. The performance of the proposed CAD system is evaluated with state-of-the-art CAD systems using various performance evaluation metrics. The experimental results showed that the proposed method can not only be used for detection but also performs well for the classification of pulmonary cancer nodules as *malignant* and *benign*.

1.2 Paper Organization

Section 2 describes our approach, Sect. 3 discusses the implementation details, Sect. 4 describes the experimental results, and Sect. 5 concludes this paper.

2 Our Approach

We improved three aspects of the lung cancer detection models. First, the datasets used by most authors do not consider the lung wall. We considered location as one of the most important features and therefore found that most nodules occur in close proximity to the lung wall. Therefore, our model avoided omitting the edge of the lung. Secondly, we used 3d U-Net to filter candidate nodules [22]. Finally, we applied CNNs for nodule classification.

2.1 Pre-processing

Our in-house dataset comprises 56 patients' CT scans using a GE CT scanner (with contrast and 3mm slice thickness) in DICOM format. Each CT scan

is composed of 80 to 200 distinct slices and the primary tumor was manually delineated using 3D-Slicer software. We resized each CT-scan data using average upsampling and average downsampling with bilinear interpolation by ImageJ software. Furthermore, we scaled the pixel value using the min-max scalar method and applied the CLAHE (Contrast Limited Adaptive Histogram Equalization) method. Data augmentation is necessary because deep learning-based models require large training datasets. The positive dataset to train our proposed model was insufficient, leading to the overfitting problem. We increased the positive dataset sample by using $128 \times 128 \times 128$ window size. We used affine transformations (rotation $[0^\circ$ to 270° around the center point], flipping, translation, and scaling) along with image enhancement by Gaussian High Pass filter with kernel size 3×3 to improve image quality and sharpening filter. For each image $P_n(z)$ shown in Eq. (1), and S in Eq. (2) where r_t , z_t is the reset and update to apply the affine transformations, respectively. While \hat{h}_t is the final augmented state of the data. The affine transformations were standardized so that the average samples have variance=1 and mean=0.

$$P_n(z) = \frac{1}{\sigma\sqrt{2\pi}} e^{-\frac{(z-\mu)^2}{2\sigma^2}} \quad (1)$$

$$S[r_t, z_t] = \Sigma_{k=-r}^n W(b, W + hr) \quad (2)$$

2.2 RPN Split-Merge Cascade Network

For the detection of various nodules having different diameters, we used varying levels of RPN_{Lx} referring to different sizes of the nodule. We set the RPN_{L1} as small anchors to detect the diameter of the nodule τ that ranges from 3 mm to 10 mm and has a volume $v \leq 80 \text{ mm}^3$ while RPN_{L2} , RPN_{L3} and RPN_{L4} have large anchors to detect nodules ranging from $\tau = 10 \text{ mm}$ – 20 mm or $v = 80$ – 200 mm^3 , $\tau = 20 \text{ mm}$ – 30 mm or $v \geq 200$ – 300 mm^3 and $\tau \geq 30 \text{ mm}$ or $v > 300 \text{ mm}^3$, respectively. The motivation behind these RPNs is the four stages of lung cancer that are categorized by different diameters, while RPN_{L1} is for all the input nodules. The RPN split and merge cascade network starts with the RPN_{L1} which is further split to either RPN_{L2} or the rest and then in the next step it is input for the RPN_{L3} or RPN_{L4} . Since each RPN level generates separate RoI sets, a merging layer is required that combines the RoI sets into one, the RPN levels merge layer RPN_m takes the input RoI sets from all the RPN levels (RPN_{L1} , RPN_{L2} , RPN_{L3} , RPN_{L4}) and outputs an aggregate RoI set RoI_{agg} . For the possibility of duplicate RoI or low objectiveness score RoI, we used the non-maxima suppression (Non-MS) when the intersection over union (IoU) overlap is above the threshold (threshold set at $\rho_t = 0.5$). After using the Non-MS, we selected the top hundred RoI with low objectiveness scores for further use. Nodule detection using different levels of RPN having various anchors improves the detection phase, as both diameter and volume are taken into consideration.

2.3 3D Residual U-Net Training Strategy and Architecture

Our proposed model relies heavily on exploiting the symmetries of the 3D space [16]. Therefore, the lung CT scan is converted into 3D fragments which are used as input for the 3D residual net. For 3D CT images containing lung nodules, the lung nodule regions were cropped to a size of $128 \times 128 \times 64$. The 3D residual net detects the module malignancy based on the characteristics obtained from the input image, and the probability of cancer stage is estimated [5]. We used binary valued threshold (corrosion & expansion) and Laplacian of Gaussian to segment the lung nodules (including lung wall), morphologic closing was performed and connected component operations are labeled in order to remove background and noise. A hole-filling algorithm based on contour information was also used to reserve the nodules on the lung wall. We obtained a collection of the interval $[x_k, y_k]$ that contains all the intervals of C_n . \mathbf{M} , so if n is large enough, $\sum_{k=1}^n |y_k - x_k| < \eta$. But $\sum_{k=1}^n |f_c(y_k) - f_c(x_k)| = 1$. The segmentation issue is addressed by taking N partitions of the set of features represented by P classes M , thus minimizing the cost term of the error function by assigning the pixel P in Eq. (3) and Eq. (4)

$$\min_{\mathbf{M}, \mathbf{x}} \sum_{i=1}^N \|\mathbf{y}_i - \mathbf{P}\mathbf{x}_i\|_2^2 \quad \text{s.t. } \forall i \|\mathbf{x}_i\|_0 \quad (3)$$

$$E = \frac{1}{2} \sum_{k=1}^N \sum_{l=1}^M R_{kl}^n V_{kl}^2 \quad (4)$$

Another challenge for our proposed model was learning the complex inner spatial relationship between parameters using deeper CNN. We added multiple residual blocks in the middle of the 3D U-Net model, which is capable of producing higher-level packet information. Taking into account the complex anatomical structures surrounding the lung lesion, we needed an effective method to use contextual information at multiple levels [15]. An overview of the CAD system for the detection of lung nodules using the 3D residual U-Net and multi-Region Proposal Network (mRPN) is shown in Fig. 1.

2.4 Malignancy Score-Based Approach (MSBA)

For the classification of detected lung lesions in the nodule detection phase, the Malignancy Score-Based Approach (MSBA) is used to achieve the assessment of nodule malignancy of candidate lesions. For this phase, the regions of interest (RoIs) that are marked by the nodule detection phase are redefined from each marked location resulting from the last step. MSBA assigns the malignancy score to RoIs by considering the metastasis information provided in the data set to classify the candidate nodule into T_0 , T_1 , T_2 , and T_3 stages. The details of MSBA are provided in Algorithm 1. The neighboring pixels in 3D surrounding the RoIs are taken into consideration in terms of intensity values and their eigenvalues (Hessian Matrix and the Gradient Matrix) to assign an aggregate score to each candidate-marked lesion. The result of this step is the allocation of the average score to all candidate nodules.

Algorithm 1. Malignancy Score-Based Approach

Require: $n + 1$ candidate nodules $(x_0, f(x_0)), (x_1, f(x_1)), \dots, (x_n, f(x_n))$
Ensure: Probability of the nodule to be pulmonary cancer nodule $P^n(x)$

```

1:  $S_{i,j} \leftarrow 0, \quad 0 \leq i, j \leq n;$ 
2:  $S_{i,j} = f[x_{i-j}, x_{i-j+1}, \dots, x_i];$ 
3: for  $i \leftarrow 0$  to  $n$  do
4:    $S_{i,0} \leftarrow f(x_i);$ 
5:   Thus,  $f(x)$  is obtained by taking the singular value decomposition;
6: end for
7: for  $i \leftarrow 1$  to  $n$  do
8:   for  $j \leftarrow 1$  to  $i$  do
9:      $S_{i,j} \leftarrow \frac{S_{i,j-1} - S_{i-1,j-1}}{x_i - x_{i-j}};$ 
10:    Sum of all the prediction values is done taking candidate nodule probability;
11:   end for
12: end for
13:  $P^n(x) \leftarrow f(x_0);$ 
14:  $R^n(x) \leftarrow 1;$ 
15: for  $i \leftarrow 1$  to  $n$  do
16:    $R^n(x) \leftarrow R^n(x) \cdot (x - x_{i-1});$ 
17:    $P^n(x) \leftarrow P^n(x) + S_{i,i} \cdot R^n(x);$ 
18: end for

```

Table 1. Confusion matrix of lung cancer classification Using 3D Residual U-Net

Stage	T0	T1	T2	T3
T0	96.24% (652)	3.32% (24)	5.84% (42)	5.96% (45)
T1	5.94% (29)	92.42% (741)	3.76% (28)	6.64% (61)
T2	10.51% (93)	7.30% (84)	91.35% (722)	3.16% (22)
T3	4.45% (18)	13.18% (102)	6.14% (54)	89.10% (709)

3 Implementation

In addition to our in-house lung cancer CT dataset, we used publicly available datasets namely the LIDC-IDRI [4], ANODE09 [8], and LUNA16 [17] for evaluation. The probability of nodules is calculated for the nodule candidates generated by the classification model. On the basis of this probability, we mark the nodules as benign and malignant in Fig. 2. To reduce false positive results, we have proposed an algorithm that considers the probability of the candidate nodule and further improves the classification of the nodules into different stages while omitting false positive results at each stage. The details of our proposed algorithm for false positive reduction are provided in Algorithm 2.

4 Experimental Results

Our results are obtained using the concept that if a detected nodule is very close to the annotated nodule, we gain a score and the score is related to the FROC curve on sensitivity at 1/8, 1/4, 1/2, 1, 2, 4, and 8 [21]. We obtained a score of 0.974 (MAX = 1) by randomly selecting data records as the test set (excluding training and validation dataset), and an accuracy of approximately 0.997 was

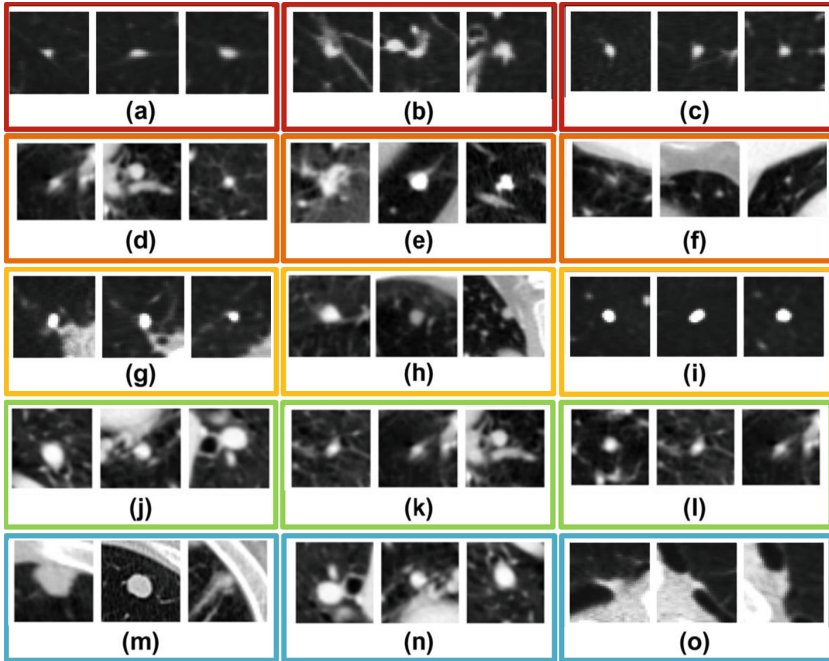


Fig. 2. Qualitative results of our proposed model on in-house dataset showing accurately detected benign nodules (T0) in (a),(b),(c); benign nodules (T1) in (d),(e),(f); malignant nodules (T2) in (g),(h),(i), malignant nodules (T3) in (j), (k) (l) and accurately detected negative nodules in (m),(n) and (o).

recorded. The results are validated using the common performance metric of computer-aided detection and diagnosis systems, i.e., average accuracy, specificity, and sensitivity. For a detailed performance analysis of our CAD system, we applied the ROC curve, which presents the TPR (True Positive Rate) as the FPR function (False Positive Rate). We plotted the sensitivity (TPR) with their respective FPR to compare our CAD system with state-of-the-art CAD systems.

The effectiveness of our method 3D Residual U-Net is verified by comparing it with Convolutional Neural Networks (CNN), Massive training artificial neural networks (MTANNs), Fully Convolutional Networks (FCN), Region-based Fully Convolutional Networks (RFCN), and RNN (Recurrent Neural Networks), the performance results are depicted in Fig. 3. Table 2 summarizes the performance of our proposed CAD system in comparison to other CAD systems in terms of accuracy, sensitivity, specificity, False Positive (FP), and average FP (using FPRA). It is visible from the confusion matrix in Table 1 that the proposed model maintains a high sensitivity for the classification of types of lung cancer even in the region where FP per scan is low. Although the proposed model achieved a high sensitivity value for stage classification for T0, T2, and T3, the sensitivity value of T1 decreases as the FP per scan becomes small, which is

Algorithm 2. False-Positive Reduction Algorithm

Require: Candidate nodule V-RoI V_{Ri} , sphericity s , ellipticity e , volume v , entropy S , maximum convergence C_{max} , intensity SD σ_I , maximum radii R_{max} , neighbors' intensity I_n

Ensure: Elimination of FPs from the candidate nodules yielding the nodules $N^P(x)$

- 1: $I_{i,j} \leftarrow 0, \quad 0 \leq i, j \leq n;$
- 2: $A_{i,j} = f[x_{i-j}, x_{i-j+1}];$
- 3: Initial Elimination Phase:
- 4: First round of Elimination of FPs from candidate nodules non-spherical and having numerous voxels;
- 5: **for** $i \leftarrow 0$ to n **do**
- 6: $V_{Ri}, 0 \leftarrow f_{ini}(x_i) = s + I_n + v;$
- 7: $f_{ini}(x)$ is obtained by sum of the sphericity, neighbors' intensity and volume;
- 8: If $f_{ini}(x_i)$ for any V-RoI $V_{Ri}, 0$ is less than the threshold T_{ini} , V-RoI is eliminated;
- 9: **end for**
- 10: Advance Elimination Phase:
- 11: **for** $i \leftarrow 1$ to n **do**
- 12: **for** $j \leftarrow 1$ to i **do**
- 13: $V_{Ri}, j \leftarrow f_{ad}(x_i) = v + s + e + S + C_{max} + \sigma_I + R_{max} + I_n;$
- 14: Eigenvalues Hessian matrix $H^i(x)$ and Gradient matrix $G^i(x);$
- 15: If $f_{ad}(x_i)$ for any V-RoI V_{Ri}, j is less than threshold T_{ad} , V-RoI is eliminated;
- 16: Features sum $f_{ad}(x)$ is done taking candidate nodule features into consideration for the classification phase;
- 17: **end for**
- 18: **end for**
- 19: Classification Phase:
- 20: $N^P(x) \leftarrow f_{cl}(x_0);$
- 21: **for** $i \leftarrow 1$ to n **do**
- 22: $N^P(x) \leftarrow N^P(i) + f_{ad}(x_i). H^n(x) + G^i(x);$
- 23: **end for**

Table 2. Performance comparison of our proposed model with state-of-the-art

Method	Accuracy	Sensitivity	Specificity	FP per scan	Avg FP (using FPRA)
CNN [23]	0.797	0.753	0.865	0.070	0.065
TumorNet [11]	0.811	0.815	0.899	0.090	0.083
FCNN [3]	0.843	0.837	0.967	0.110	0.071
DFCNet [13]	0.967	0.821	0.954	0.040	0.029
mRFCN [14]	0.913	0.731	0.864	0.063	0.034
Ours	0.997	0.976	0.942	0.045	0.026

impractical in the clinical environment [14]. A summary of our proposed CAD system in terms of stage classification is shown in Table 1. The experimental results demonstrate the superiority in the classification and class generalization of our proposed 3D Residual U-Net based CAD system. A comparison of nodule classification by CAD systems is shown in Fig. 4.

A comparison of our model with the existing state-of-the-art CADE systems on the LIDC-IDRI dataset with varying nodule sizes is shown in Table 3. We have compared the detection accuracy of our CADE system with the detection accuracy of five other existing systems, which are evaluated on the dataset from the LIDC-IDRI database. The high accuracy of our proposed model with varying sizes signifies the detection capability of our 3D Residual U-Net model. Our method has promising results in discriminating cancer nodule types without compromising detection accuracy (Fig. 4).

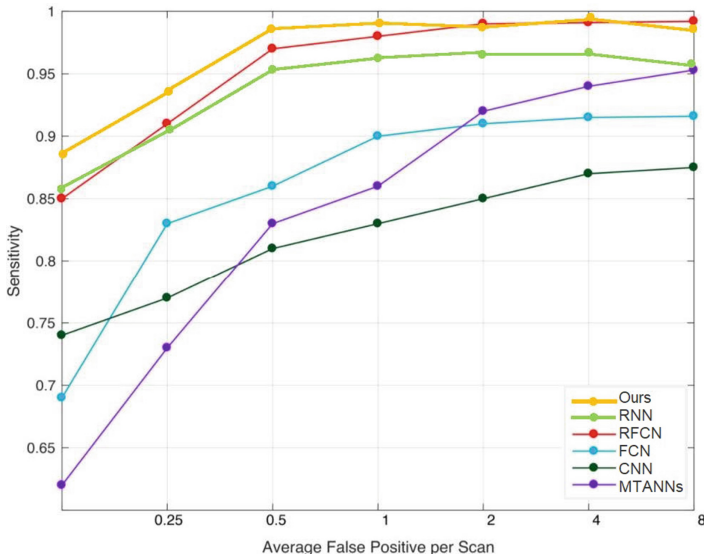


Fig. 3. The plot illustrating the sensitivity of the 3D residual model on the Luna16 dataset with the state-of-the-art CAD systems. The x -axis denotes the average number of FP per scan while the y -axis represents the sensitivity.

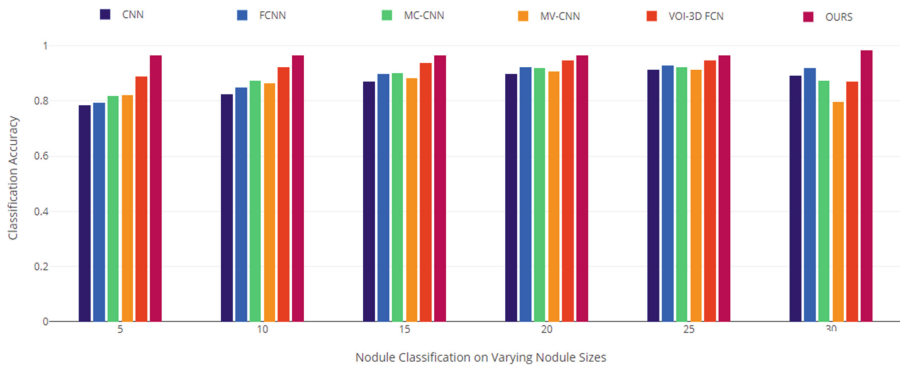


Fig. 4. Comparison of our 3D residual U-Net CAD system nodule classification with state-of-the-art CAde systems.

Table 3. Comparison of our proposed model on nodule classification with the state-of-the-art CADe systems using CT dataset (subset of inhouse data, LIDC-IDRI [4], ANODE09 [8], LUNA16)

Model	<= 3 mm	5 mm	10 mm	20 mm	30 mm	>30 mm	Avg ACC*
CNN [20]	0.67	0.78	0.86	0.91	0.88	0.85	0.83
FCNN and SVM [7]	0.75	0.79	0.77	0.91	0.92	0.93	0.73
Multi-Crop CNN [18]	0.68	0.81	0.90	0.89	0.87	0.91	0.85
Multi-View CNN [16]	0.67	0.81	0.86	0.90	0.91	0.87	0.84
VOI Based 3D-FCN [9]	0.90	0.88	0.93	0.94	0.87	0.96	0.91
Ours(3D Residual U-Net)	0.94	0.96	0.96	0.97	0.98	0.98	0.96

* Avg ACC means Average Accuracy; Row 2 to Row 7 represent different nodule sizes

5 Conclusion

We proposed a novel CAD system for the automatic detection and classification of lung nodules in CT images. Our CAD system comprises two models, the 3D residual U-Net and multi-Region Proposal Network (mRPN), which have demonstrated effective nodule detection results even with small-sized lesions. For the classification of nodules, the aggregate malignancy score is calculated for each detected nodule. Based on this score, detected nodules are classified into four classes; T_0 , T_1 , T_2 , and T_3 . Experimental results illustrate the efficacy of our proposed CAD system in comparison to state-of-the-art CAD systems that use various performance evaluation metrics. Our proposed CAD system is generic and therefore could possibly be extended to the detection of other cancers.

References

1. Adams, S.J., Stone, E., Baldwin, D.R., Vliegenthart, R., Lee, P., Fintelmann, F.J.: Lung cancer screening. *Lancet* **401**(10374), 390–408 (2023)
2. Alahmari, S.S., Cherezov, D., Goldgof, D.B., Hall, L.O., Gillies, R.J., Schabath, M.B.: Delta radiomics improves pulmonary nodule malignancy prediction in lung cancer screening. *IEEE Access* **6**, 77796–77806 (2018)
3. Alves, J.H., Neto, P.M.M., Oliveira, L.F.: Extracting lungs from ct images using fully convolutional networks. In: 2018 International Joint Conference on Neural Networks (IJCNN), pp. 1–8. IEEE (2018)
4. Armato, S.G., III.: The lung image database consortium (LIDC) and image database resource initiative (IDRI): a completed reference database of lung nodules on CT scans. *Med. Phys.* **38**(2), 915–931 (2011)
5. Dou, Q., Chen, H., Yu, L., Qin, J., Heng, P.A.: Multilevel contextual 3-D CNNs for false positive reduction in pulmonary nodule detection. *IEEE Trans. Biomed. Eng.* **64**(7), 1558–1567 (2017)
6. Firmino, M., Angelo, G., Morais, H., Dantas, M.R., Valentim, R.: Computer-aided detection (CADe) and diagnosis (CADx) system for lung cancer with likelihood of malignancy. *BioMed. Eng. OnLine* **15**(1), 2:1–2:17 (2016)

7. van Ginneken, B., Setio, A.A.A., Jacobs, C., Ciompi, F.: Off-the-shelf convolutional neural network features for pulmonary nodule detection in computed tomography scans. In: IEEE International Symposium on Biomedical Imaging, pp. 286–289 (2015)
8. van Ginneken, B., et al.: Comparing and combining algorithms for computer-aided detection of pulmonary nodules in computed tomography scans: the ANODE09 study. *Med. Image Anal.* **14**(6), 707–722 (2010)
9. Hamidian, S., Sahiner, B., Petrick, N., Pezeshk, A.: 3D convolutional neural network for automatic detection of lung nodules in chest CT. In: Proceedings of SPIE, vol. 10134 (2017)
10. Huang, S., Yang, J., Shen, N., Xu, Q., Zhao, Q.: Artificial intelligence in lung cancer diagnosis and prognosis: current application and future perspective. In: Seminars in Cancer Biology. Elsevier (2023)
11. Hussein, S., Gillies, R., Cao, K., Song, Q., Bagci, U.: TumorNet: lung nodule characterization using multi-view convolutional neural network with Gaussian process. In: IEEE International Symposium on Biomedical Imaging, pp. 1007–1010 (2017)
12. Li, X., Deng, Z., Deng, Q., Zhang, L., Niu, T., Kuang, Y.: A novel deep learning framework for internal gross target volume definition from 4d computed tomography of lung cancer patients. *IEEE Access* **6**, 37775–37783 (2018)
13. Masood, A., et al.: Computer-assisted decision support system in pulmonary cancer detection and stage classification on CT images. *J. Biomed. Inf.* **79**, 117–128 (2018)
14. Masood, A., et al.: Automated decision support system for lung cancer detection and classification via enhanced rfcn with multilayer fusion rpn. *IEEE Trans. Ind. Inf.* **16**(12), 7791–7801 (2020)
15. Masood, A., et al.: Cloud-based automated clinical decision support system for detection and diagnosis of lung cancer in chest CT. *IEEE J. Transl. Eng. Health Med.* **8**, 1–13 (2019)
16. Setio, A.A.A., et al.: Pulmonary nodule detection in CT images: false positive reduction using multi-view convolutional networks. *IEEE Trans. Med. Imaging* **35**(5), 1160–1169 (2016)
17. Setio, A.A.A., et al.: Validation, comparison, and combination of algorithms for automatic detection of pulmonary nodules in computed tomography images: The LUNA16 challenge. *Med. Image Anal.* **42**, 1–13 (2017)
18. Shen, W., et al.: Multi-crop convolutional neural networks for lung nodule malignancy suspiciousness classification. *Pattern Recogn.* **61**, 663–673 (2017)
19. Siegel, R.L., Miller, K.D., Wagle, N.S., Jemal, A.: Cancer statistics, 2023. *Ca Canc. J. Clin.* **73**(1), 17–48 (2023)
20. Tan, M., Deklerck, R., Jansen, B., Bister, M., Cornelis, J.: A novel computer-aided lung nodule detection system for CT images. *Med. Phys.* **38**(10), 5630–5645 (2011)
21. Teramoto, A., Fujita, H.: Fast lung nodule detection in chest CT images using cylindrical nodule-enhancement filter. *Int. J. Comput. Assist. Radiol. Surg.* **8**(2), 193–205 (2013)
22. Xie, Y., Zhang, J., Xia, Y., Fulham, M., Zhang, Y.: Fusing texture, shape and deep model-learned information at decision level for automated classification of lung nodules on chest CT. *Inf. Fusion* **42**, 102–110 (2018)
23. Yuan, J., Liu, X., Hou, F., Qin, H., Hao, A.: Hybrid-feature-guided lung nodule type classification on CT images. *Comput. Graph.* **70**, 288–299 (2018)